Quantum Spin Dynamics Due to Strong Kitaev Interactions in the Triangular-Lattice Antiferromagnet $CsCeSe_2$

Tao Xie,[1,2,*,†] S. Gozel,[3,*] Jie Xing,[4] N. Zhao,[5] S. M. Avdoshenko,[6] L. Wu,[7] Athena S. Sefat,[4] A. L. Chernyshev,[8] A. M. Läuchli,[3,9] A. Podlesnyak,[2] and S. E. Nikitin[10,‡]

[1]*Center for Neutron Science and Technology, Guangdong Provincial Key Laboratory of Magnetoelectric Physics and Devices, School of Physics, Sun Yat-sen University, Guangzhou, Guangdong 510275, China*
[2]*Neutron Scattering Division, Oak Ridge National Laboratory, Oak Ridge, Tennessee 37831, USA*
[3]*Laboratory for Theoretical and Computational Physics, Paul Scherrer Institute, CH-5232 Villigen-PSI, Switzerland*
[4]*Materials Science and Technology Division, Oak Ridge National Laboratory, Oak Ridge, Tennessee 37831, USA*
[5]*Department of Physics, Southern University of Science and Technology, Shenzhen, Guangdong 518055, China*
[6]*Leibniz-Institut für Festkörper- und Werkstoffforschung (IFW Dresden), Helmholtzstraße 20, 01069 Dresden, Germany*
[7]*Department of Physics and Academy for Advanced Interdisciplinary Studies, Southern University of Science and Technology, Shenzhen, Guangdong 518055, China*
[8]*Department of Physics and Astronomy, University of California, Irvine, California 92697, USA*
[9]*Institute of Physics, Ecole Polytechnique Fédérale de Lausanne (EPFL), CH-1015 Lausanne, Switzerland*
[10]*Laboratory for Neutron Scattering and Imaging, Paul Scherrer Institut, CH-5232 Villigen-PSI, Switzerland*

(Received 27 November 2023; revised 13 June 2024; accepted 22 July 2024; published 29 August 2024)

The extraordinary properties of the Kitaev model have motivated an intense search for new physics in materials that combine geometrical and bond frustration. In this Letter, we employ inelastic neutron scattering, spin wave theory, and exact diagonalization to study the spin dynamics in the perfect triangular-lattice antiferromagnet (TLAF) $CsCeSe_2$. This material orders into a stripe phase, which is demonstrated to arise as a consequence of the off-diagonal bond-dependent terms in the spin Hamiltonian. By studying the spin dynamics at intermediate fields, we identify an interaction between the single-magnon state and the two-magnon continuum that causes decay of coherent magnon excitations, level repulsion, and transfer of spectral weight to the continuum that are controlled by the strength of the magnetic field. Our results provide a microscopic mechanism for the stabilization of the stripe phase in TLAF and show how complex many-body physics can be present in the spin dynamics in a magnet with strong Kitaev coupling even in an ordered ground state.

DOI: 10.1103/PhysRevLett.133.096703

Introduction—In the quantum theory of solids, elementary excitations can be described as emergent entities known as quasiparticles [1,2]. Noninteracting quasiparticles have infinite lifetime and well-defined dispersion in the momentum-energy space. Interaction between quasiparticles can reduce their lifetime via decays, renormalize their dispersion, and even drive phase transitions [3,4]. Magnetic insulating systems provide ideal platforms for investigating interactions between the quasiparticles, because of their relative simplicity and purity [5]. Magnetic Hamiltonians in such systems are usually dominated by several nearest-neighbor (NN) couplings [6], and can often be determined with good fidelity [7]. Moreover, the magnetic field provides a clear nonthermal control parameter to tune the ground state of the system [8].

The magnon-magnon interaction can be restricted by the high symmetry of the system [9], making materials with anisotropic-exchange interactions especially appealing. Because of the lattice symmetry, the NN exchange matrix of a triangular-lattice antiferromagnet (TLAF) is parameterized by four parameters: isotropic exchange J, XXZ anisotropy Δ, and two bond-dependent (BD) terms, $J_{\pm\pm}$ and $J_{z\pm}$ [10,11], as we will detail below. Notably, a linear combination of $J_{\pm\pm}$ and $J_{z\pm}$ constitutes the best known BD interactions—the celebrated Kitaev term, $KS_i^\alpha S_j^\alpha$ ($\alpha \in \{x, y, z\}$) [12–14]. The phase diagram of the BD TLAF has been characterized by analytical and numerical methods [11,15–18] and is summarized in Fig. 1(a) for $\Delta = 1/4$. It can be divided into regions of the stripe-x, stripe-yz, and 120° order, depending on the sign of $J_{\pm\pm}$ and the value of $J_{z\pm}$. In addition, a U(1) quantum spin-liquid

*These authors contributed equally to this work.
†Contact author: xiet69@mail.sysu.edu.cn
‡Contact author: stanislav.nikitin@psi.ch

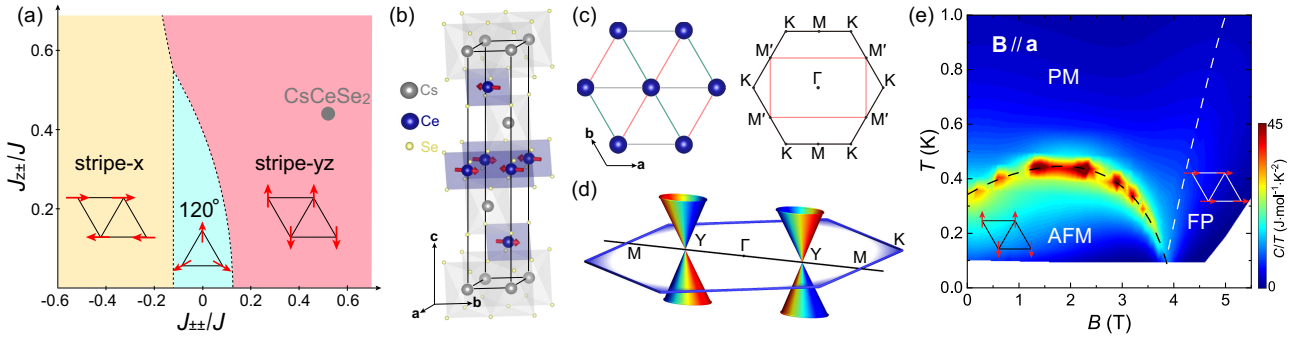

FIG. 1. (a) Zero-temperature phase diagram of the NN $S = 1/2$ TLAF (1) with $\Delta = 1/4$ [17]. In the stripe-x phase, spins lie in the ab plane, parallel to the bonds, while in the stripe-yz phase, they point perpendicular to the bonds and can be canted out of the ab plane. (b) Crystal and magnetic structure of $CsCeSe_2$. The red arrows represent magnetic moments of Ce^{3+}. (c) Left: projection of the lattice on the ab plane with three different bonds marked by different colors. Right: crystallographic (black) and magnetic (red) BZ of $CsCeSe_2$. (d) Schematic representation of Dirac cones at the Y points, where magnons cross due to the symmetry of the stripe-yz state. (e) Magnetic B-T phase diagram [19]. The black dashed line represents the phase boundary between the AFM and paramagnetic (PM) or field-polarized (FP) phase. The white dashed line indicates a crossover between the PM and FP phases.

(QSL) phase has been suggested between the 120° and stripe phases for $0.7 \lesssim \Delta \lesssim 1$ [17].

Such Kitaev-like BD terms arise naturally in magnets with strong spin-orbit coupling [20,21] when the total multiplet of a magnetic ion is projected onto the low-energy pseudo-$S = 1/2$ model. However, the experimental realizations of such terms remain very rare [22,23]. Rare-earth delafossites represent a promising playground for the studies of TLAF because of their distortion-free crystal structure with well-separated triangular layers [24,25]. Yb-based materials are known to potentially possess QSL [26–29] or the 120° ordered states [30,31], while Ce [32–34] and Er [35,36]-based materials order into the stripe phases [Fig. 1(b)] because of the BD terms. However, there has been no report on the anomalous spin dynamics caused by the BD terms in these materials until now.

Here, we focus on $CsCeSe_2$ that orders magnetically into the stripe-yz phase below $T_N = 0.35$ K [19]. A combination of crystalline electric field and spin-orbit coupling splits the $J = 5/2$ multiplet of Ce^{3+} into three well-separated Kramers doublets, with the groundstate doublet corresponding to an effective $S = 1/2$ [19,37]. Application of the magnetic field, $\mathbf{B}||\mathbf{a}$, suppresses the stripe order at a potential quantum critical point and stabilizes the field-polarized (FP) state [Fig. 1(e)]. We collect inelastic neutron scattering (INS) spectra at all relevant fields and our results reveal the anomalous spin excitations in the ordered stripe and FP phases. Using these data we refine the spin Hamiltonian and establish that the BD terms are responsible for the stabilization of the stripe-yz order. Our INS spectra and exact diagonalization (ED) calculations demonstrate a large broadening of the spectra at intermediate fields and complete breakdown of magnons at the Γ point of the Brillouin zone (BZ) just below the critical field ($B_c = 3.86$ T). We also find strong repulsion between the single magnon branch and the two-magnon continuum (TMC) that is best visible at the Y point of the BZ. Our results unravel the crucial role of the magnon-magnon interaction induced by the BD terms in modifying the excitation spectrum of the TLAF with a magnetically ordered ground state.

Spin dynamics in $CsCeSe_2$—$CsCeSe_2$ orders into the two-sublattice stripe-yz phase [Fig. 2(a)] which breaks the C_3 lattice symmetry [19]. The corresponding magnetic BZ is nested in the crystallographic one [Fig. 1(c)]. As a consequence, the otherwise-equivalent high-symmetry points of the BZ become nonequivalent. Below we label the two M points associated with the ordering wave vector as M and the four others as M' [Fig. 1(c)].

Figure 2(b) shows the INS spectrum at zero field. Its primary feature is a sharp intense excitation at the Γ point. Away from the zone center, $CsCeSe_2$ exhibits three spin-wave branches: one nearly gapless acoustic and two weakly dispersive optical modes. The canted stripe-yz order has two magnetic sublattices and, in the spin-wave approximation, $CsCeSe_2$ should feature two magnon modes at $B < B_c$. However, in zero field $CsCeSe_2$ is in a multidomain state, and, therefore, the INS spectrum consists of the superposition of three domains, $I(\mathbf{Q}, \hbar\omega) = I(\mathbf{Q}_{\Gamma\longrightarrow M}, \hbar\omega) + 2I(\mathbf{Q}_{\Gamma\longrightarrow M'}, \hbar\omega)$. This increases the number of modes up to six, but the two pairs of these modes, originating from the domains ordered at the M' points, are exactly degenerate along the $\Gamma \longrightarrow M$ path.

Application of the magnetic field selects one domain with the ordering wave vector $\mathbf{q}\perp\mathbf{B}$, and the spectra obtained at 1.4 (see Supplemental Material (SM) [39]) and 2.3 T [Fig. 2(c)] yield a weakly dispersive mode around 0.35 meV [56]. At 3 T [Fig. 2(d)] the spectrum exhibits qualitative modifications: the mode becomes more dispersive and the excitation at the Γ point strongly broadens in energy [Fig. 2(g)]. At 4 T the spectrum demonstrates a low-energy dispersive mode and an arch-shaped resonancelike

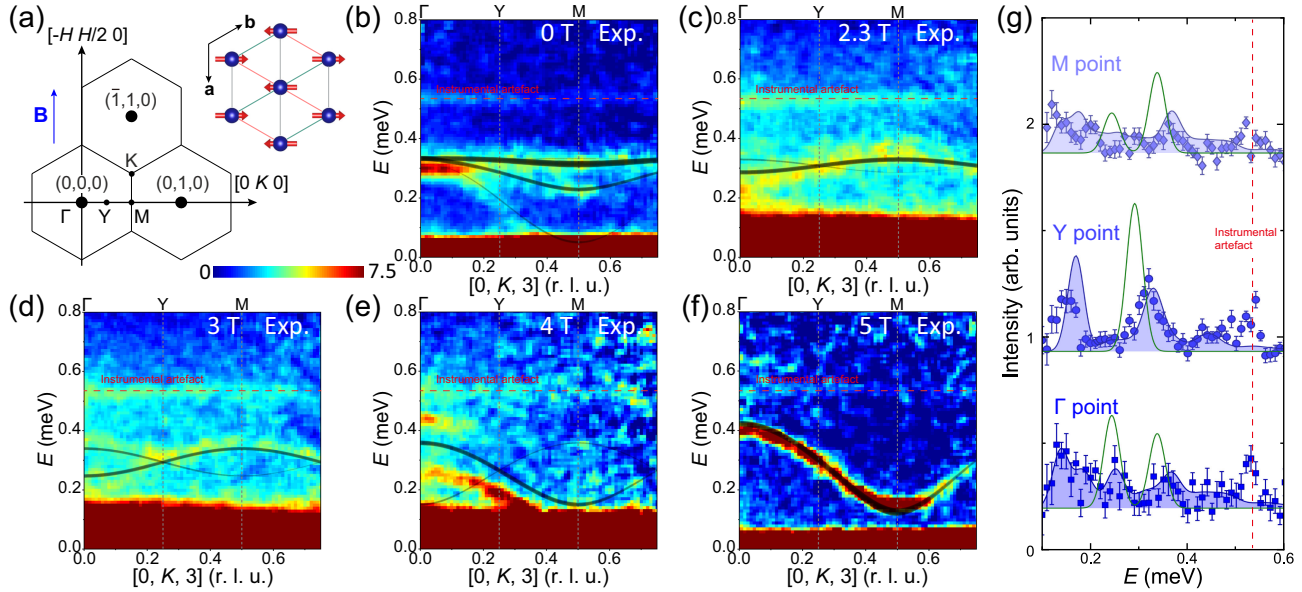

FIG. 2. (a) Left: representation of the BZ in the $(H\,K\,0)$ plane. The blue arrow indicates the magnetic field direction. Right: projection of the Ce^{3+} moments on the ab plane at zero field. (b)–(f) Comparisons of the experimental spectra with results of the LSWT calculations at different magnetic fields. All INS data were taken at $T = 70$ mK and integrated by ± 2.5 r.l.u. along $[0\,0\,L]$ and ± 0.1 r.l.u. along $[H\,-H/2\,0]$ directions. The black lines on the top of color maps are the mode positions and intensities given by LSWT. (g) Comparison between the INS data and calculations at different $\mathbf{Q}$ points and $B = 3$ T [38]. The shadow areas are ED and the green curves are the LSWT results, respectively. The red dashed lines in panels (b)–(g) indicate the instrumental artifact ≈0.54 meV.

feature at $E \approx 0.45$ meV, which is localized at a close proximity of the Γ point [Fig. 2(e)]. The intensity distribution over the low-energy mode is not homogeneous and it weakens close to the Γ point, just below the high-energy arch. Further increase of the field stabilizes the FP state and the spectrum exhibits a sharp mode with a cosinelike dispersion [Fig. 2(f)]. We note that in the high-field regime, $B \geq 5$ T, the observed excitations are resolution limited, but broaden considerably in the lower fields [39].

Now we turn to the determination of the Hamiltonian parameters. The spin Hamiltonian for the NN triangular lattice reads as [10,11,15,17,57]

$$\mathcal{H} = \sum_{\langle ij \rangle} \mathbf{S}_i^{\mathrm{T}} \hat{\mathbf{J}}_{ij} \mathbf{S}_j - \mu_B g_{ab} B \sum_i S_i^x \qquad (1)$$

where μ_{B} is the Bohr magneton, g_{ab} is the in-plane g factor, B is the magnetic field, and $\hat{\mathbf{J}}_{ij}$ is the exchange matrix, defined as

$$\hat{\mathbf{J}}_{ij} = \begin{pmatrix} J + 2J_{\pm\pm} & 0 & 0 \\ 0 & J - 2J_{\pm\pm} & J_{z\pm} \\ 0 & J_{z\pm} & \Delta J \end{pmatrix}, \qquad (2)$$

for the bond along the **a** axis, which transforms according to the lattice symmetry for the other bonds [11]. The Hamiltonian (1) has five independent variables, which we determine by fitting the dispersion in the high-field regime and using calculations of the low-field spectral response using ED as is detailed in the SM [39]. Our results safely exclude considerable next-NN interactions, and the best fit yields $J = 72.5$ μeV, $\Delta = 0.25$, $J_{\pm\pm}/J = 0.52$, $J_{z\pm}/J = 0.41$, and $g_{ab} = 1.77$ [58,60]. These parameters put $CsCeSe_2$ deep into the stripe-yz phase of the general phase diagram of the TLAF [Fig. 1(a)] and demonstrate that the stripe order is stabilized by a combination of the strong BD terms.

We note that the linear spin-wave theory (LSWT) and symmetry consideration [61] suggest the Dirac crossing in the magnon spectrum at the Y points [Fig. 1(d)]. While the presence of the magnon-magnon interaction may suggest some exotic interplay of it with the Dirac topology [62,63], our results presented below are unable to support such a scenario.

The LSWT calculations of the spin wave for each field are summarized in Figs. 2(b)–2(f). Clearly, LSWT captures perfectly the high-field data and reproduces some features of the *dispersion* in the low-field regime, $B \leq 2.3$ T, with semiquantitative accuracy. However, accurate comparison of the intensities clearly demonstrates that at intermediate field regime $0 < B < B_{\mathrm{c}}$, the LSWT simulations do not provide an adequate description of the observed data despite the presence of robust magnetic order [19]. To show that, in Fig. 2(g) we plot the INS data taken at 3 T at the Γ, Y, and M points together with LSWT and ED results. According to the LSWT, the spectra at the Γ and M points contain two sharp modes in clear contrast with the INS

data, which exhibit a very broad response with only a weak hint of the LSWT-predicted modes, indicating magnon breakdown due to strong magnon-magnon interactions. Moreover, the LSWT spectrum at the Y point features a single mode due to topological protection, while our data clearly show the two-peak structure, providing strong evidence that a more sophisticated treatment is required.

To provide an accurate description of the observed INS data, we utilize unbiased numerical ED calculations on a finite system size up to $N = 32$ spins. We note that the spectral function computed with ED and LSWT are converted to the INS cross section taking into account all relevant factors [39]. This allows us to make quantitative comparisons between INS and ED at three high-symmetry points (Γ, Y, and M) of the BZ.

First, we consider the spectrum measured at 4 T that contains the high-energy arch near the Γ point [Fig. 3(a)]. This field is just above B_c [19], and, based on the LSWT, one would expect a resolution-limited magnon branch. Indeed, our INS data show the presence of a sharp low-energy magnon branch which, however, strongly broadens close to the Γ point. The INS spectrum can be reproduced by the nonlinear SWT calculation with a semiquantitative accuracy. It reproduces the high-energy arch around the Γ point that can be observed clearly, despite its weaker intensity [Fig. 3(a)]. Our Fig. 3(b) shows the single-magnon dispersion and the lower boundary of the TMC versus field obtained by ED [39]. One can see that the broadening of the single-magnon branch takes place when the magnon branch enters the TMC. Such an overlap makes the decay of the single magnon kinematically allowed below ≈5.5 T and explains the momentum-dependent broadening of the magnon mode. Our ED calculations clearly support this scenario and also reproduce the formation of the high-energy resonance feature, which we interpret as a large density of states within the TMC.

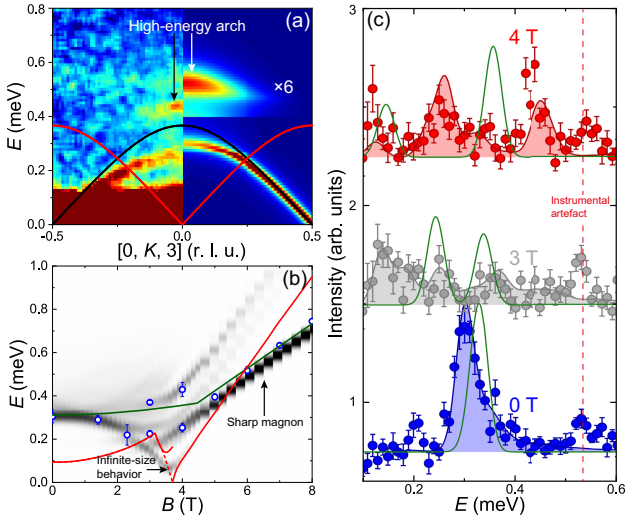

FIG. 3. (a) The INS spectrum of $CsCeSe_2$ collected at 4 T (left) compared with nonlinear SWT calculations (right). The black line is the LSWT dispersion and the red line is the bottom of the TMC at 4 T. The arrows point to the high-energy "arch" within the TMC. The intensity of the upper part of the calculated spectrum ($E > 0.4$ meV) is multiplied by ×6 for better visual clarity. (b) Calculated dynamical structure factor at the Γ point and different fields obtained using ED. The blue open circles are experimental results. The dark green line is the LSWT results. The red line is the lower boundary of the TMC. (c) Comparisons of the experimental and the calculated spin excitation spectra at the Γ point [38]. The shadow areas are ED calculations, and the green curves are LSWT results.

At B_c, the TMC extends to vanishing energy at the Γ point [64]. This causes a strong broadening of the magnetic signal at the spectra collected at 2.3 and 3 T where the experimental spectral weight is smoothly distributed between 0.1 and 0.4 meV indicating a complete breakdown of the single-magnon excitation. In contrast, a relatively sharp Lorentzian-shaped mode is formed at lower fields, see Fig. 3(b). While the LSWT captures some parts of the spectral response at 0 T, it fails in the intermediate field regime, while ED reproduces our INS data with a high accuracy at all relevant fields, see Fig. 3(c). We speculate that the failure of the LSWT at intermediate fields is expected because the spectra are subject to stronger quantum effects for the canted, noncollinear spin configuration. That allows for a stronger coupling between the longitudinal and transverse spin excitations via the three-magnon processes, opening up additional channels for magnon decays [9].

Now we turn to the description of the data collected at the Y point. As we discussed above, the LSWT predicts a topologically protected Dirac point in the stripe-yz phase. Thus, the spectrum at the Y point should feature one mode at every field above zero. However, the magnon-magnon interaction induces strong modifications of the spectrum. Figures 4(a) and 4(b) show the ED-calculated INS spectra at different fields. In the FP regime, $B > B_c$, it shows a sharp mode that exhibits a nonmonotonic behavior in the ordered phase $B < B_c$: first it bends up just below B_c, qualitatively similar to the predictions of LSWT. However, at $B \approx 2.5$ T it twists in the opposite direction. Moreover, most of the spectral weight at low fields is transferred from this mode to the high-energy continuum at 0.3–0.4 meV. Notably, the position of the intense excitation at low fields agrees quantitatively with the LSWT predictions.

To rationalize the origin of such a behavior we calculate the lower boundary of the TMC at the Y point using ED, shown by the red line in Fig. 4(b). The low-energy mode is located just below the lower edge of the TMC. Such a behavior is caused by a repulsion between the single-magnon branch and the continuum in the avoided quasiparticle decay scenario [65,66]. Our INS data support this scenario and show two well-separated INS peaks at 3 T, see Fig. 4(c). In our setup, we can control and track the strength of the repulsion by applying a magnetic field, in contrast to

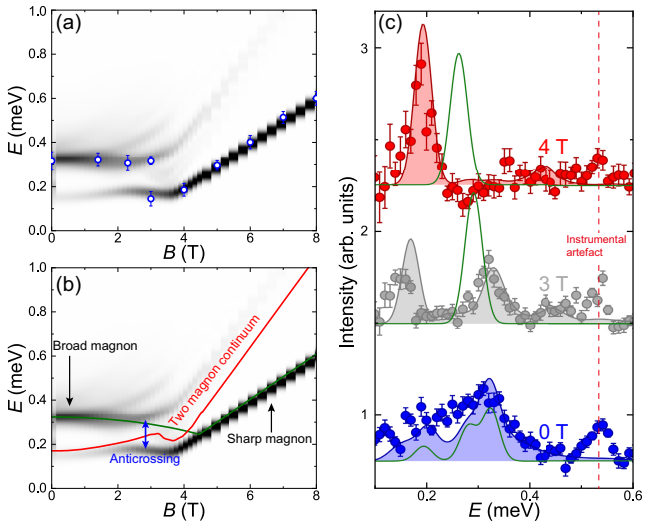

FIG. 4. (a) Dynamical structure factor of $CsCeSe_2$ calculated by ED. The blue open circles are experimental results. (b) A replica of the ED calculations in panel (a) with different regions indicated with single magnon and TMC. The dark green line is LSWT calculations. The red line is the lower boundary of the TMC. The blue arrow emphasizes the anticrossing behavior between the single-magnon branch and the TMC. (c) Comparisons of the experimental and the calculated spectra at Y point [38]. The shadow areas are ED calculations, and the green curves are LSWT results.

that in Ref. [66], where the repulsion is manifested as a function of the momentum transfer.

Discussion and conclusion—The interaction between a quasiparticle branch and a continuum has two opposite regimes: when the interaction is weak, the quasiparticle acquires a finite lifetime where the mode enters the continuum. In the case of strong interactions, a level repulsion scenario can take place, meaning that the quasiparticle dispersion will repel from the continuum remaining sharp in energy. Our spectroscopic study of $CsCeSe_2$ demonstrates the presence of both effects which arise as a consequence of interactions between the single-magnon branches and the multimagnon continuum. This interaction has substantial matrix elements because of the sizable bond-dependent terms, $J_{\pm\pm}$ and $J_{z\pm}$, in the spin Hamiltonian and, furthermore, its effect can be controlled by a magnetic field. Specifically, using the 4 T dataset we demonstrate that once the single-magnon branch enters the TMC, it exhibits downward renormalization and acquires a finite lifetime, in agreement with the weak-interacting scenario, while part of the spectral weight is transferred to the TMC. The spectra at the Γ point at 2.3 T and 3 T show a very broad response indicating a complete breakdown of the single-magnon excitation which, however, is almost reestablished in the collinear zero-field phase.

The data collected at the Y point demonstrate anticrossinglike behavior, where the single-magnon branch is repelled by the lower boundary of the TMC, remaining relatively sharp in energy. This behavior is induced by a strong interaction between the magnon branch and the continuum, which was observed previously in the excitation spectrum of liquid ^{4}He and in the TLAF Heisenberg magnet [66–70]. Our results are essential for the understanding of the many-body spin dynamics in materials that combine geometrical and bond frustration.

Acknowledgments—We thank Dr. Hongtao Liu (Instrument Analysis & Research Center, Sun Yat-sen University) for the assistance with LA-ICP-TOF measurements and data evaluations. We thank Dr. Jong Keum for the help with the x-ray Laue and x-ray diffraction measurements, Dr. Feng Ye for assistance with single-crystal x-ray diffraction measurements, N. D. Andriushin for the help with figure preparations, Dr. Jörg Sichelschmidt for the attempts of the ESR measurements and the helpful discussion. Work at Sun Yat-sen University was supported by the National Natural Science Foundation of China (Grant No. 12304187), the open research fund of Songshan Lake Materials Laboratory (Grant No. 2023SLABFN30), the Guangzhou Basic and Applied Basic Research Funds (Grant No. 2024A04J4024), and the Fundamental Research Funds for the Central Universities, Sun Yat-sen University (Grant No. 23qnpy57). Work at Oak Ridge National Laboratory (ORNL) was supported by the U.S. Department of Energy (DOE), Office of Science, Basic Energy Sciences, Materials Science and Engineering Division. This research used resources at the Spallation Neutron Source, a DOE Office of Science User Facility operated by the Oak Ridge National Laboratory. X-ray Laue and XRD measurements were conducted at the Center for Nanophase Materials Sciences (CNMS) (CNMS2019-R18) at ORNL, which is a DOE Office of Science User Facility. The work of A. L. C. on the analytical SWT was supported by the U.S. Department of Energy, Office of Science, Basic Energy Sciences under Award No. DE-SC0021221.

[1] A. Prabhakar and D. D. Stancil, *Spin Waves: Theory and Applications* (Springer, New York, 2009), Vol. 5.
[2] A. Borovik-Romanov and S. Sinha, Introduction, in *Spin Waves and Magnetic Excitations, Modern Problems in Condensed Matter Sciences* Vol. 22, edited by A. Borovik-Romanov and S. Sinha (Elsevier, New York, 1988), pp. xi–xxviii.
[3] C. W. Li, J. Hong, A. F. May, D. Bansal, S. Chi, T. Hong, G. Ehlers, and O. Delaire, Orbitally driven giant phonon anharmonicity in SnSe, Nat. Phys. **11**, 1063 (2015).
[4] J. Hong and O. Delaire, Phase transition and anharmonicity in SnSe, Mater. Today Phys. **10**, 100093 (2019).
[5] D. S. Inosov, Quantum magnetism in minerals, Adv. Phys. **67**, 149 (2018).
[6] K. W. H. Stevens, Exchange interactions in magnetic insulators, Phys. Rep. **24**, 1 (1976).

[7] A. Vasiliev, O. Volkova, E. Zvereva, and M. Markina, Milestones of low-D quantum magnetism, npj Quantum Mater. **3**, 18 (2018).

[8] T. Giamarchi, C. Rüeggn, and O. Tchernyshyov, Bose–Einstein condensation in magnetic insulators, Nat. Phys. **4**, 198 (2008).

[9] M. E. Zhitomirsky and A. L. Chernyshev, Colloquium: Spontaneous magnon decays, Rev. Mod. Phys. **85**, 219 (2013).

[10] Y. Li, G. Chen, W. Tong, L. Pi, J. Liu, Z. Yang, X. Wang, and Q. Zhang, Rare-Earth triangular lattice spin liquid: A single-crystal study of $YbMgGaO_4$, Phys. Rev. Lett. **115**, 167203 (2015).

[11] P. A. Maksimov, Z. Zhu, S. R. White, and A. L. Chernyshev, Anisotropic-exchange magnets on a triangular lattice: Spin waves, accidental degeneracies, and dual spin liquids, Phys. Rev. X **9**, 021017 (2019).

[12] P. A. Maksimov, Z. Zhu, S. R. White, and A. L. Chernyshev, Erratum: Anisotropic-exchange magnets on a triangular lattice: Spin waves, accidental degeneracies, and dual spin liquids, Phys. Rev. X **12**, 019902(E) (2022).

[13] A. Kitaev, Anyons in an exactly solved model and beyond, Ann. Phys. (N.Y.) **321**, 2 (2006).

[14] C. Liu, Y.-D. Li, and G. Chen, Selective measurements of intertwined multipolar orders: Non-Kramers doublets on a triangular lattice, Phys. Rev. B **98**, 045119 (2018).

[15] Y.-D. Li, X. Wang, and G. Chen, Anisotropic spin model of strong spin-orbit-coupled triangular antiferromagnets, Phys. Rev. B **94**, 035107 (2016).

[16] Q. Luo, S. Hu, B. Xi, J. Zhao, and X. Wang, Ground-state phase diagram of an anisotropic spin-$\frac{1}{2}$ model on the triangular lattice, Phys. Rev. B **95**, 165110 (2017).

[17] Z. Zhu, P. A. Maksimov, S. R. White, and A. L. Chernyshev, Topography of spin liquids on a triangular lattice, Phys. Rev. Lett. **120**, 207203 (2018).

[18] M. Wu, D.-X. Yao, and H.-Q. Wu, Exact diagonalization study of the anisotropic Heisenberg model related to $YbMgGaO_4$, Phys. Rev. B **103**, 205122 (2021).

[19] T. Xie, N. Zhao, S. Gozel, J. Xing, S. M. Avdoshenko, K. M. Taddei, A. I. Kolesnikov, L. D. Sanjeewa, Peiyue Ma, N. Harrison, C. dela Cruz, L. Wu, A. S. Sefat, A. L. Chernyshev, A. M. Läuchli, A. Podlesnyak, and S. E. Nikitin, companion paper, Stripe magnetic order and field-induced quantum criticality in the perfect triangular-lattice antiferromagnet $CsCeSe_2$, Phys. Rev. B **110**, 054445 (2024).

[20] F.-Y. Li, Y.-D. Li, Y. Yu, A. Paramekanti, and G. Chen, Kitaev materials beyond iridates: Order by quantum disorder and Weyl magnons in rare-earth double perovskites, Phys. Rev. B **95**, 085132 (2017).

[21] H. Takagi, T. Takayama, G. Jackeli, G. Khaliullin, and S. E. Nagler, Concept and realization of Kitaev quantum spin liquids, Nat. Rev. Phys. **1**, 264 (2019).

[22] K. E. Avers, P. A. Maksimov, P. F. S. Rosa, S. M. Thomas, J. D. Thompson, W. P. Halperin, R. Movshovich, and A. L. Chernyshev, Fingerprinting triangular-lattice antiferromagnet by excitation gaps, Phys. Rev. B **103**, L180406 (2021).

[23] C. Kim, S. Kim, P. Park, T. Kim, J. Jeong, S. Ohira-Kawamura, N. Murai, K. Nakajima, A. L. Chernyshev, M. Mourigal, S.-J. Kim, and S.-G. Park, Bond-dependent anisotropy and magnon decay in cobalt-based Kitaev triangular antiferromagnet, Nat. Phys. **19**, 1624 (2023).

[24] W. Liu, Z. Zhang, J. Ji, Y. Liu, J. Li, X. Wang, H. Lei, G. Chen, and Q. Zhang, Rare-Earth chalcogenides: A large family of triangular lattice spin liquid candidates, Chin. Phys. Lett. **35**, 117501 (2018).

[25] M. Baenitz, P. Schlender, J. Sichelschmidt, Y. A. Onykiienko, Z. Zangeneh, K. M. Ranjith, R. Sarkar, L. Hozoi, H. C. Walker, J.-C. Orain, H. Yasuoka, J. van den Brink, H. H. Klauss, D. S. Inosov, and T. Doert, $NaYbS_2$: A planar spin-$\frac{1}{2}$ triangular-lattice magnet and putative spin liquid, Phys. Rev. B **98**, 220409(R) (2018).

[26] L. Ding, P. Manuel, S. Bachus, F. Grußler, P. Gegenwart, J. Singleton, R. D. Johnson, H. C. Walker, D. T. Adroja, A. D. Hillier, and A. A. Tsirlin, Gapless spin-liquid state in the structurally disorder-free triangular antiferromagnet $NaYbO_2$, Phys. Rev. B **100**, 144432 (2019).

[27] M. Bordelon, E. Kenney, T. Hogan, L. Posthuma, M. Kavand, Y. Lyu, M. Sherwin, C. Brown, M. Graf, L. Balents, and S. D. Wilson, Field-tunable quantum disordered ground state in the triangular lattice antiferromagnet $NaYbO_2$, Nat. Phys. **15**, 1058 (2019).

[28] J. Xing, L. D. Sanjeewa, J. Kim, G. R. Stewart, A. Podlesnyak, and A. S. Sefat, Field-induced magnetic transition and spin fluctuations in the quantum spin-liquid candidate $CsYbSe_2$, Phys. Rev. B **100**, 220407(R) (2019).

[29] P.-L. Dai *et al.*, Spinon Fermi surface spin liquid in a triangular lattice antiferromagnet $NaYbSe_2$, Phys. Rev. X **11**, 021044 (2021).

[30] T. Xie, A. A. Eberharter, J. Xing, S. Nishimoto, M. Brando, P. Khanenko, J. Sichelschmidt, A. A. Turrini, D. G. Mazzone, P. G. Naumov, L. D. Sanjeewa, N. Harrison, A. S. Sefat, B. Normand, A. M. Läuchli, A. Podlesnyak, and S. E. Nikitin, Complete field-induced spectral response of the spin-1/2 triangular-lattice antiferromagnet $CsYbSe_2$, npj Quantum Mater. **8**, 48 (2023).

[31] A. O. Scheie, E. A. Ghioldi, J. Xing, J. A. M. Paddison, N. E. Sherman, M. Dupont, D. Abernathy, D. M. Pajerowski, S.-S. Zhang, L. O. Manuel, A. E. Trumper, C. D. Pemmaraju, A. S. Sefat, D. S. Parker, T. P. Devereaux, J. E. Moore, C. D. Batista, and D. A. Tennant, Witnessing quantum criticality and entanglement in the triangular antiferromagnet $KYbSe_2$, Nat. Phys. **20**, 74 (2024).

[32] G. Bastien *et al.*, Long-range magnetic order in the $\tilde{S} = 1/2$ triangular lattice antiferromagnet $KCeS_2$, SciPost Phys. **9**, 041 (2020).

[33] A. A. Kulbakov, S. M. Avdoshenko, I. Puente-Orench, M. Deeb, M. Doerr, P. Schlender, T. Doert, and D. S. Inosov, Stripe-yz magnetic order in the triangular-lattice antiferromagnet $KCeS_2$, J. Phys. Condens. Matter **33**, 425802 (2021).

[34] S. M. Avdoshenko, A. A. Kulbakov, E. Häußler, P. Schlender, T. Doert, J. Ollivier, and D. S. Inosov, Spin-wave dynamics in the $KCeS_2$ delafossite: A theoretical description of powder inelastic neutron-scattering data, Phys. Rev. B **106**, 214431 (2022).

[35] J. Xing, K. M. Taddei, L. D. Sanjeewa, R. S. Fishman, M. Daum, M. Mourigal, C. dela Cruz, and A. S. Sefat, Stripe antiferromagnetic ground state of the ideal triangular lattice compound $KErSe_2$, Phys. Rev. B **103**, 144413 (2021).

[36] G. Ding, H. Wo, R. L. Luo, Y. Gu, Y. Gu, R. Bewley, G. Chen, and J. Zhao, Stripe order and spin dynamics in triangular-lattice antiferromagnet $KErSe_2$: A single-crystal study with a theoretical description, Phys. Rev. B **107**, L100411 (2023).

[37] Y.-D. Li, X. Wang, and G. Chen, Hidden multipolar orders of dipole-octupole doublets on a triangular lattice, Phys. Rev. B **94**, 201114(R) (2016).

[38] The background was subtracted from the INS data as detailed in Sec. S1B of SM [39].

[39] See Supplemental Material at http://link.aps.org/supplemental/10.1103/PhysRevLett.133.096703 for details on the INS measurements, ED calculations, linear and nonlinear SWT calculations, and on the procedure of fitting of exchange interactions. The Supplemental Material includes Refs. [11,19,22,40–55].

[40] J. Xing, L. D. Sanjeewa, J. Kim, G. R. Stewart, M.-H. Du, F. A. Reboredo, R. Custelcean, and A. S. Sefat, Crystal synthesis and frustrated magnetism in triangular lattice $CsRESe_2$ (RE = La-Lu): Quantum spin liquid candidates $CsCeSe_2$ and $CsYbSe_2$, ACS Mater. Lett. **2**, 71 (2020).

[41] G. Ehlers, A. Podlesnyak, J. L. Niedziela, E. B. Iverson, and P. E. Sokol, The new cold neutron chopper spectrometer at the spallation neutron source: Design and performance, Rev. Sci. Instrum. **82**, 085108 (2011).

[42] G. Ehlers, A. Podlesnyak, and A. I. Kolesnikov, The cold neutron chopper spectrometer at the Spallation Neutron Source—A review of the first 8 years of operation, Rev. Sci. Instrum. **87**, 093902 (2016).

[43] O. Arnold, J. C. Bilheux, J. M. Borreguero, A. Buts, S. I. Campbell, L. Chapon, M. Doucet, N. Draper, R. F. Leal, M. A. Gigg *et al.*, Mantid—Data analysis and visualization package for neutron scattering and μSR experiments, Nucl. Instrum. Methods Phys. Res., Sect. A **764**, 156 (2014).

[44] R. A. Ewings, A. Buts, M. D. Le, J. van Duijn, I. Bustinduy, and T. G. Perring, HORACE: Software for the analysis of data from single crystal spectroscopy experiments at time-of-flight neutron instruments, Nucl. Instrum. Methods Phys. Res., Sect. A **834**, 3132 (2016).

[45] S. Toth and B. Lake, Linear spin wave theory for single-Q incommensurate magnetic structures, J. Phys. Condens. Matter **27**, 166002 (2015).

[46] J. Xing, L. D. Sanjeewa, J. Kim, G. R. Stewart, M.-H. Du, F. A. Reboredo, R. Custelcean, and A. S. Sefat, CSD 1952065: Experimental Crystal Structure Determination, 10.25505/fiz.icsd.cc23j8vs (2020).

[47] N. Navid, Mag2pol: A program for the analysis of spherical neutron polarimetry, flipping ratio and integrated intensity data, J. Appl. Crystallogr. **52**, 175 (2019).

[48] A. S. Wills, A new protocol for the determination of magnetic structures using simulated annealing and representational analysis (SARAh), Physica (Amsterdam) **276B**, 680 (2000).

[49] Y. Ohta, T. Shimozato, R. Eder, and S. Maekawa, Bogoliubov quasiparticle excitations in the two-dimensional t-j model, Phys. Rev. Lett. **73**, 324 (1994).

[50] D. Poilblanc, D. J. Scalapino, and S. Capponi, Superconducting gap for a two-leg $t - j$ ladder, Phys. Rev. Lett. **91**, 137203 (2003).

[51] Y.-D. Li, Y. Shen, Y. Li, J. Zhao, and G. Chen, Effect of spin-orbit coupling on the effective-spin correlation in $YbMgGaO_4$, Phys. Rev. B **97**, 125105 (2018).

[52] R. L. Smit, S. Keupert, O. Tsyplyatyev, P. A. Maksimov, A. L. Chernyshev, and P. Kopietz, Magnon damping in the zigzag phase of the Kitaev-Heisenberg-Γ model on a honeycomb lattice, Phys. Rev. B **101**, 054424 (2020).

[53] A. L. Chernyshev and M. E. Zhitomirsky, Spin waves in a triangular lattice antiferromagnet: Decays, spectrum renormalization, and singularities, Phys. Rev. B **79**, 144416 (2009).

[54] A. Lüscher and A. M. Läuchli, Exact diagonalization study of the antiferromagnetic spin-1/2 Heisenberg model on the square lattice in a magnetic field, Phys. Rev. B **79**, 195102 (2009).

[55] M. E. Zhitomirsky and A. L. Chernyshev, Instability of antiferromagnetic magnons in strong fields, Phys. Rev. Lett. **82**, 4536 (1999).

[56] The second mode is primarily polarized along the **c** axis, and its intensity is strongly suppressed due to the anisotropy of the g factor.

[57] Y.-D. Li, Y. Shen, Y. Li, J. Zhao, and G. Chen, Effect of spin-orbit coupling on the effective-spin correlation in $YbMgGaO_4$, Phys. Rev. B **97**, 125105 (2018).

[58] Equivalently, these parameters can be written using J-K-Γ-Γ′ notations [11,12,59]: $J = -82.5$ μeV, $K = -33.3$ μeV, $\Gamma = -65.5$ μeV and $\Gamma' = 14$ μeV. This indicates that J and Γ are the leading terms and the Kitaev interaction K is of the same order as the leading terms.

[59] P. A. Maksimov and A. L. Chernyshev, Easy-plane anisotropic-exchange magnets on a honeycomb lattice: Quantum effects and dealing with them, Phys. Rev. B **106**, 214411 (2022).

[60] As detailed in the SM, these values of the couplings should be understood as a representative set of couplings rather than an "exact" estimate.

[61] M. J. Karaki, X. Yang, A. J. Williams, M. Nawwar, V. Doan-Nguyen, J. E. Goldberger, and Y.-M. Lu, An efficient material search for room-temperature topological magnons, Sci. Adv. **9**, eade7731 (2023).

[62] P. A. McClarty and J. G. Rau, Non-Hermitian topology of spontaneous magnon decay, Phys. Rev. B **100**, 100405(R) (2019).

[63] A. Mook, K. Plekhanov, J. Klinovaja, and D. Loss, Interaction-stabilized topological magnon insulator in ferromagnets, Phys. Rev. X **11**, 021061 (2021).

[64] In ED, this is only true in the thermodynamic limit.

[65] K. W. Plumb, K. Hwang, Y. Qiu, L. W. Harriger, G. E. Granroth, A. I. Kolesnikov, G. J. Shu, F. C. Chou, C. Rüegg, Y. B. Kim, and Y.-J. Kim, Quasiparticle-continuum level repulsion in a quantum magnet, Nat. Phys. **12**, 224 (2016).

[66] R. Verresen, R. Moessner, and F. Pollmann, Avoided quasiparticle decay from strong quantum interactions, Nat. Phys. **15**, 750 (2019).

[67] R. J. Donnelly, J. A. Donnelly, and R. N. Hills, Specific heat and dispersion curve for helium II, J. Low Temp. Phys. **44**, 471 (1981).

[68] H. R. Glyde, M. R. Gibbs, W. G. Stirling, and M. A. Adams, Excitations in superfluid ^{4}He beyond the roton, Europhys. Lett. **43**, 422 (1998).

[69] H. Godfrin, K. Beauvois, A. Sultan, E. Krotscheck, J. Dawidowski, B. Fåk, and J. Ollivier, Dispersion relation of Landau elementary excitations and thermodynamic properties of superfluid ^{4}He, Phys. Rev. B **103**, 104516 (2021).

[70] D. Macdougal, S. Williams, D. Prabhakaran, R. I. Bewley, D. J. Voneshen, and R. Coldea, Avoided quasiparticle decay and enhanced excitation continuum in the spin-$\frac{1}{2}$ near-Heisenberg triangular antiferromagnet $Ba_3CoSb_2O_9$, Phys. Rev. B **102**, 064421 (2020).